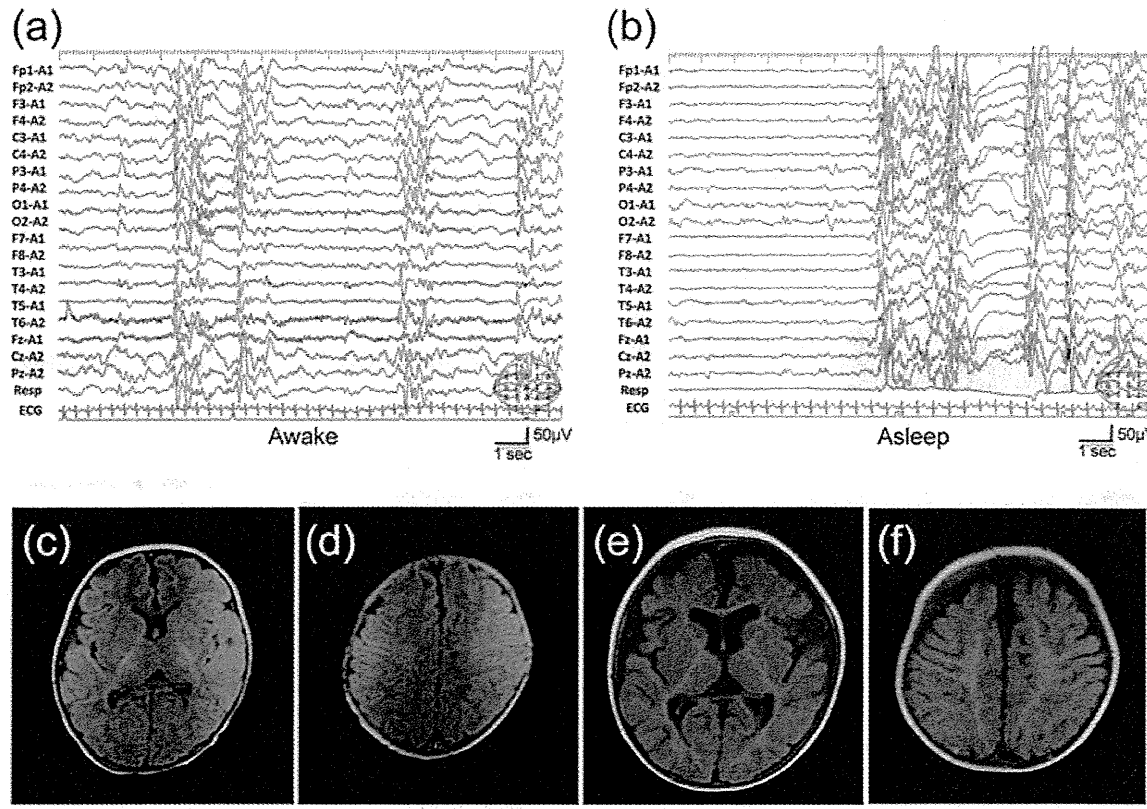

Fig. 1. Interictal electroencephalogram (EEG) (**a**, **b**) and brain magnetic resonance imaging (MRI) (**c**–**f**) of the patient. EEG during both waking (**a**) and sleep (**b**) at 1 month of age showed suppression-burst pattern consisting of low-voltage, almost flat phase and high-voltage paroxysmal activity phase. Brain MRI showed normal findings at 1 month of age (**c**, **d**), and slightly dilated lateral ventricles at 11 months of age (**e**, **f**) because of adrenocorticotropic hormone injection.

could affect donor splicing of exon 10, reverse transcriptase (RT)–PCR designed to amplify exons 9–12 was performed using total RNA extracted from LCL derived from the patient (Fig. 2a). A single band (286 bp), corresponding to the wild-type *STXBP1* allele, was amplified using a cDNA template from a control LCL (Fig. 2b). By contrast, a longer band was detected from the patient's cDNA (Fig. 2b). The longer mutant transcript had a 138-bp insertion of intron 10 sequences (Fig. 2c), producing a premature stop codon at amino acid position 302; therefore, the mutant mRNAs are probably to be degraded by NMD (11, 12). The intensity ratio of the mutant compared to the normal band was increased up to 36.3% after treatment with 30 μM cycloheximide, which inhibits NMD, compared to 13.8% in the untreated condition (Fig. 2d). Thus the mutant transcript suffered from degradation by NMD, which would result in haploinsufficiency of *STXBP1*.

To examine whether the c.902+5G>A mutation occurred *de novo*, the parental DNA extracted from whole blood were analyzed by HRM. Compared with the mother's sample, the patient's sample showed clearly shifted melting curve, indicating that the heterozygous c.902+5G>A mutation could be surely detected (Fig. 3a). Interestingly, the father's sample showed a slightly shifted melting curve, suggesting that the father may harbor the mutation in mosaic state, which was suggested by sequencing (Fig. 3a,b). Similar melting curves and electropherograms were obtained in DNA extracted from saliva, buccal cells, and nails (Fig. 3a,b). We further investigated the mosaicism by counting wild-type G and mutant A alleles after TA cloning of the PCR product. DNA extracted from blood, saliva, buccal cells, and nails suggested that 5.3%, 8.7%, 11.9%, and 16.9% of alleles (i.e. 10.6%, 17.4%, 23.8%, and 33.8% of cells) harbored the mutation, respectively (Fig. 3c).

Discussion

To date, 13 point mutations and one deletion of *STXBP1* have been reported in individuals with OS (9, 10). Thirteen out of fourteen deletion/mutations were confirmed as *de novo*

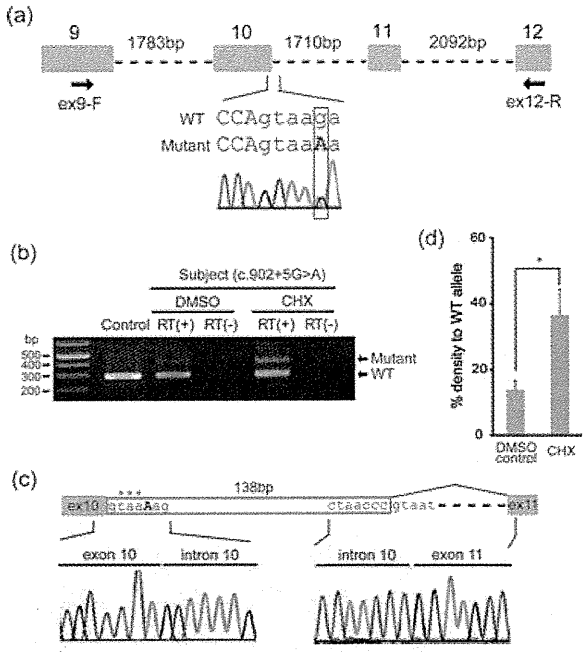

Fig. 2. The c.902+5G>A mutation causing abnormal splicing associated with nonsense-mediated mRNA decay (NMD). (**a**) Schematic representation of the genomic structure from exons 9 to 12 of *STXBP1*. Exons, introns and primers are shown by gray boxes, dashed lines and arrows, respectively. The mutation in intron 10 was colored in red. Sequences of exon and intron are presented in upper and lower cases, respectively. (**b**) Reverse transcriptase (RT) – PCR analysis of the patient with c.902+5G>A and a normal control. Two PCR products were detected from the patient's cDNA: lower was the wild-type (WT) transcript and upper was the mutant. Only a single WT amplicon was detected in a control. The mutant amplicon was significantly increased by 30-μM cycloheximide (CHX) treatment compared to DMSO treatment as a vehicle control. RT (+): with reverse transcriptase, RT (−): without reverse transcriptase as a negative control. (**c**) Sequence of mutant amplicons clearly showed a 138-bp insertion of intron 10 sequences and a premature stop codon (asterisk) in the mutant transcript. (**d**) Quantitative analysis of the NMD inhibition by CHX based on the data shown in (**b**). *p = 0.00186 by unpaired Student's *t*-test (two-tailed). Averages of duplicated experiments using two distinctive RNA samples, respectively, are shown with error bars (standard deviation).

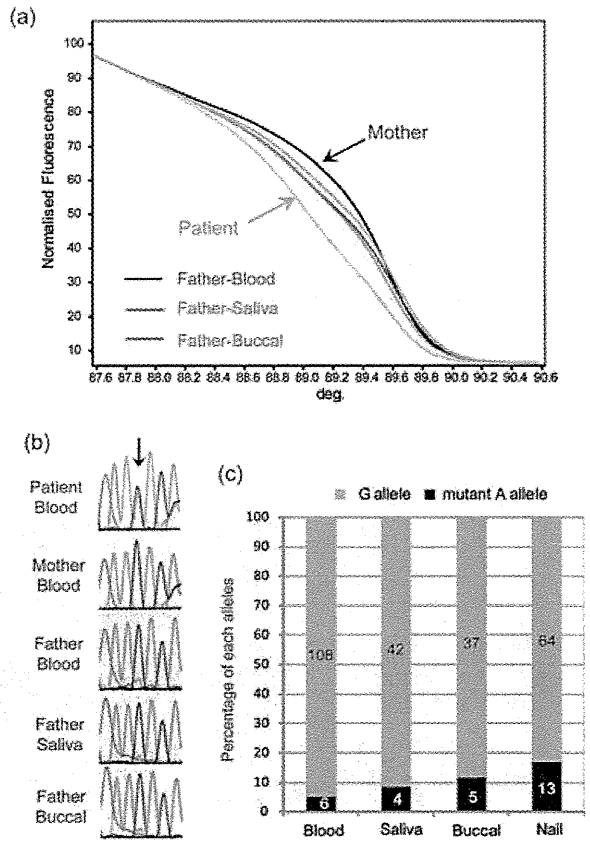

Fig. 3. Paternal somatic mosaicism of the c.902+5G>A mutation. (**a**) Melting curves of PCR products. Compared with the mother's sample (black), the patient's sample (gray) showed largely shifted melting curve. The father's sample from blood (red), saliva (green), and buccal cells (blue) showed slightly, but distinctly shifted melting curves. (**b**) Electropherograms of the c.902+5G>A mutation (arrow) showed mosaicism of the mutation in the father. (**c**) Allele frequencies counted by TA cloning of PCR products and sequencing. DNA extracted from blood, saliva, buccal cells, and nails of the father showed that 5.3%, 8.7%, 11.9%, and 16.9% of alleles harbored the mutant A allele. The numbers of colonies corresponding to each allele are indicated within bars.

events (paternal DNA was unavailable for one remaining mutation). Many OSs are sporadic, probably because of their poor outcome with severe psychomotor retardation; however, some X-linked familial cases have been reported with *ARX* mutations (6, 8). Here we have showed a paternal somatic mosaicism of an *STXBP1* mutation. Although DNA from the semen of the father could not be analyzed in this study, the identical c.902+5G>A mutation found in both the father and the affected daughter indicated that the father should possess the mutation in germ cells as a mosaic state, suggesting recurrence risks. Thus, somatic and germline mosaicism of *STXBP1* mutations should be carefully taken into account especially for genetic counseling of familial OS cases.

We have successfully identified the paternal somatic mosaicism of an *STXBP1* mutation by HRM. DNA from blood indicated that the mosaic ratio is as low as about 5%; therefore, HRM could be very sensitive in detecting low-ratio mosaicism. HRM is a rapid and simple approach to detect heteroduplexes (13). It only requires the addition of a saturating dye before PCR. By HRM analysis of the PCR products, the sensitivity of successful detection of heterozygotes is nearly 100% (13). It should be noted that the sensitivity of HRM to

detect somatic changes or heteroplasmy is much better than that of DNA sequencing (14, 15): HRM could detect the level of somatic mosaicism down to 5–10% (15). However, the ability to detect low percentage heterodeuplex of PCR products may vary among mutations. Although the heterozygous c.902+5G>A mutation showed largely shifted melting curve, we experienced some heterozygous mutations only showing slightly shifted melting curve, in which we may not be able to detect the mosaicism. Therefore, optimization of HRM analysis for each mutation would be recommended especially to examine parental samples.

In conclusion, we firstly described the paternal somatic mosaicism of an *STXBP1* mutation. The percentage of mosaicism was quite low (5–17%), and no minor problems like dexterity, intelligence (cognition), behavior or psychological state were recognized in the father. The information described here was quite useful for future genetic counseling of this family.

Acknowledgements

We would like to thank the patient and her family for their participation in this study. This work was supported by Research Grants from the Ministry of Health, Labour and Welfare (N. M. and M. K.), Grant-in-Aid for Scientific Research from Japan Society for the Promotion of Science (N. M. and M. K.), Grant-in-Aid for Young Scientist from Japan Society for the Promotion of Science (H. S.), Research Promotion Fund from Yokohama Foundation for Advancement of Medical Science (H. S.), Research Grants from the Japan Epilepsy Research Foundation (H. S. and M. K.), and Research Grant from Naito Foundation (N. M.).

References

1. Ohtahara S, Ishida T, Oka E et al. On the specific age dependent epileptic syndrome: the early-infantile epileptic encephalopathy with suppression-burst. No to Hattatsu 1976: 8: 270–279.
2. Djukic A, Lado FA, Shinnar S et al. Are early myoclonic encephalopathy (EME) and the Ohtahara syndrome (EIEE) independent of each other?. Epilepsy Res 2006: 70 (Suppl. 1): S68–S76.
3. Ohtahara S, Yamatogi Y. Ohtahara syndrome: with special reference to its developmental aspects for differentiating from early myoclonic encephalopathy. Epilepsy Res 2006: 70 (Suppl. 1): S58–S67.
4. Yamatogi Y, Ohtahara S. Early-infantile epileptic encephalopathy with suppression-bursts, Ohtahara syndrome; its overview referring to our 16 cases. Brain Dev 2002: 24: 13–23.
5. Kato M, Saitoh S, Kamei A et al. A Llonger Ppolyalanine Eexpansion Mmutation in the ARX Ggene Ccauses Eearly Iinfantile Eepileptic Eencephalopathy with Ssuppression-Bburst Ppattern (Ohtahara Ssyndrome). Am J Hum Genet 2007: 81: 361–366.
6. Fullston T, Brueton L, Willis T et al. Ohtahara syndrome in a family with an ARX protein truncation mutation (c.81C>G/p.Y27X). Eur J Hum Genet 2010: 18: 157–162.
7. Absoud M, Parr JR, Halliday D et al. A novel ARX phenotype: rapid neurodegeneration with Ohtahara syndrome and a dyskinetic movement disorder. Dev Med Child Neurol 2009: 52: 305–307.
8. Kato M, Koyama N, Ohta M et al. Frameshift mutations of the ARX gene in familial Ohtahara syndrome. Epilepsia 2010: 51: 1679–1684.
9. Saitsu H, Kato M, Mizuguchi T et al. *De novo* mutations in the gene encoding STXBP1 (MUNC18-1) cause early infantile epileptic encephalopathy. Nat Genet 2008: 40: 782–788.
10. Saitsu H, Kato M, Okada I et al. STXBP1 mutations in early infantile epileptic encephalopathy with suppression-burst pattern. Epilepsia, doi: 10.1111/j.1528-1167.2010.02728.x.
11. Shyu AB, Wilkinson MF, van Hoof A. Messenger RNA regulation: to translate or to degrade. EMBO J 2008: 27: 471–481.
12. Maquat LE, Kinniburgh AJ, Rachmilewitz EA et al. Unstable beta-globin mRNA in mRNA-deficient beta o thalassemia. Cell 1981: 27: 543–553.
13. Wittwer CT. High-resolution DNA melting analysis: advancements and limitations. Hum Mutat 2009: 30: 857–859.
14. Dobrowolski SF, Hendrickx AT, van den Bosch BJ et al. Identifying sequence variants in the human mitochondrial genome using high-resolution melt (HRM) profiling. Hum Mutat 2009: 30: 891–898.
15. Vossen RH, Aten E, Roos A et al. High-resolution melting analysis (HRMA): more than just sequence variant screening. Hum Mutat 2009: 30: 860–866.

CLINICAL REPORT

AMERICAN JOURNAL OF medical genetics PART A

A De Novo Deletion of 20q11.2–q12 in a Boy Presenting With Abnormal Hands and Feet, Retinal Dysplasia, and Intractable Feeding Difficulty

Yoko Hiraki,[1,2] Akira Nishimura,[2] Michiko Hayashidani,[3] Yoshiko Terada,[4] Gen Nishimura,[5] Nobuhiko Okamoto,[6] Sachiko Nishina,[7] Yoshinori Tsurusaki,[2] Hiroshi Doi,[2] Hirotomo Saitsu,[2] Noriko Miyake,[2] and Naomichi Matsumoto[2]*

[1]Hiroshima Municipal Center for Child Health and Development, Hiroshima, Japan

[2]Department of Human Genetics, Yokohama City University Graduate School of Medicine, Yokohama, Japan

[3]Medical Center for Premature and Neonatal Infants, Hiroshima City Hospital, Hiroshima, Japan

[4]Department of Ophthalmology, Hiroshima City Hospital, Hiroshima, Japan

[5]Department of Pediatric Imaging, Tokyo Metropolitan Children's Medical Center, Tokyo, Japan

[6]Department of Medical Genetics, Osaka Medical Center and Research Institute for Maternal and Child Health, Osaka, Japan

[7]Department of Ophthalmology, National Center for Child Health and Development, Tokyo, Japan

Received 18 June 2010; Accepted 23 October 2010

Proximal interstitial deletions involving 20q11–q12 are very rare. Only two cases have been reported. We describe another patient with 20q11.21–q12 deletion. We precisely mapped the 6.5-Mb deletion and successfully determined the deletion landmarks at the nucleotide level. Common clinical features among the three cases include developmental delay, intractable feeding difficulties with gastroesophageal reflux, and facial dysmorphism including triangular face, hypertelorism, and hypoplastic alae nasi, indicating that the 20q11.2–q12 deletion can be a clinically recognizable syndrome. This is also supported by the fact that the three deletions overlap significantly. In addition, unique features such as arthrogryposis/fetal akinesia (hypokinesia) deformation and retinal dysplasia are recognized in the patient reported herein. © 2011 Wiley-Liss, Inc.

Key words: 20q interstitial deletion; abnormal hands and feet; retinal dysplasia; feeding difficulty

How to Cite this Article:
Hiraki Y, Nishimura A, Hayashidani M, Terada Y, Nishimura G, Okamoto N, Nishina S, Tsurusaki Y, Doi H, Saitsu H, Miyake N, Matsumoto N. 2011. A de novo deletion of 20q11.2–q12 in a boy presenting with abnormal hands and feet, retinal dysplasia, and intractable feeding difficulty.
Am J Med Genet Part A 155:409–414.

INTRODUCTION

Interstitial deletions of the long arm of chromosome 20 are rare. To our knowledge, a total of 12 patients have been reported in the literature [Petersen et al., 1987; Shabtai et al., 1993; Aldred et al., 2002; Genevieve et al., 2005; Callier et al., 2006; Borozdin et al., 2007; Iqbal and Al-Owain, 2007]. Among them, only two cases showed the proximal q deletion (20q11–q12), not extending to q13 [Callier et al., 2006; Iqbal and Al-Owain, 2007]. One patient had a 6.6-Mb deletion at 20q11.21–q11.23 [Callier et al., 2006], and the other [Iqbal and Al-Owain, 2007] showed a 6.8-Mb deletion at 20q11.2–q12. Here, we report on the third patient with a 6.5-Mb deletion at 20q11.21–q12, clinically showing mental retardation, minor craniofacial anomalies, and intractable feeding difficulties. The deletion has been precisely analyzed at the nucleotide level and his detailed clinical manifestations will be presented.

Grant sponsor: Japan Society for the Promotion of Science (JSPS); Grant sponsor: Ministry of Health, Labour and Welfare; Grant sponsor: Ministry of Education, Culture, Sports, Science and Technology of Japan; Grant sponsor: Scientific Research.

*Correspondence to:
Naomichi Matsumoto, Department of Human Genetics, Yokohama City University Graduate School of Medicine, Fukuura 3-9, Kanazawa-ku, Yokohama 236-0004, Japan. E-mail: naomat@yokohama-cu.ac.jp

Published online 11 January 2011 in Wiley Online Library (wileyonlinelibrary.com).
DOI 10.1002/ajmg.a.33818

CLINICAL REPORT

The 18-month-old boy was the first product of healthy 22-year-old mother and 25-year-old father without any consanguinity. Pregnancy was uneventful. Family history was unremarkable. He was born by spontaneous vaginal delivery at 38 weeks of gestation. Birth weight was 2,230 g (−1.7 SD), length 44.0 cm (−1.9 SD), and OFC 32.5 cm (−0.3 SD). Multiple malformations including patent ductus arteriosus, patency of foramen ovale, and dysmorphic face were noted. He was tube-fed due to poor swallowing and oxygen therapy was required until 4 months because of respiratory disturbance. X-ray examination at age of 1 month revealed small thorax and mild slender long bones. In addition, right eye retinal fold was pointed out. At age of 3 months, upper gastrointestinal tract was investigated because of recurrent vomiting, and gastroesophageal reflux (GER) and esophageal hiatus hernia were found. Esophageal hiatus hernia was alleviated spontaneously, but GER persisted.

At age of 4 months, he was referred to us for evaluation of his developmental delay. He was noted to have the following craniofacial features: triangular face, premature closure fontanelle, slopping forehead, wide bending eyebrows, hypertelorism, low-set and posterior rotated ears, long columella nasi, mild hypoplastic alae nasi, short and well-defined philtrum, thin lips with tucked-in lower lip, submucosal cleft palate, microretrognathia and posterior low hair-line (Fig. 1A,B and Table I). Additionally, abnormal hands and feet were recognized, consisted of restriction of all proximal interphalangeal joints and over-extension of all distal interphalangeal joints of hands and feet, radial deviation of 2nd fingers, clinodactyly of the 2nd and 5th fingers, lack of flexion creases bilaterally, right preaxial polydactyly, left single palmar, and talipes valgus. Mild restriction of elbow, hip and knee joints bilaterally was also noted (Fig. 1C–E and Table I).

At 15 months, his weight was 7.5 kg (−2.3 SD), length 71.8 cm (−2.7 SD), and OFC 44.4 cm (−1.6 SD). He could roll over one side and shift a toy from one hand to the other. Social smile was seen, but he could not recognize his parents (DQ 48). His dysphagia persisted based on the modified swallowing study [Kanda et al., 2005]; he required tube-feeding, and rejected oral intake. Ophthalmic examination at 15 months revealed broom-like pattern of retinal vessels extending from optic disc to periphery with a falciform retinal fold in the right eye, causing visual impairment. In the left eye, mild opacity in the lateral portion of vitreous body was found. These findings led to the diagnosis of bilateral retinal dysplasia. Anterior segment and optic disc were normal. Left hearing loss was suspected by auditory brainstem response, otoacoustic emission, and behavioral observation audiometry. Brain magnetic resonance imaging revealed cortical atrophy and mild ventriculomegaly. Blood biochemistry and abdominal ultrasonographic examination were all normal. Serological TORCH (toxoplasma, rubella, cytomegarovirus, and herpes simplex) testing was negative. At 18 months, the shortening of 5th middle phalanges of fingers and absence of middle phalanges of the toes were confirmed by X-ray examination.

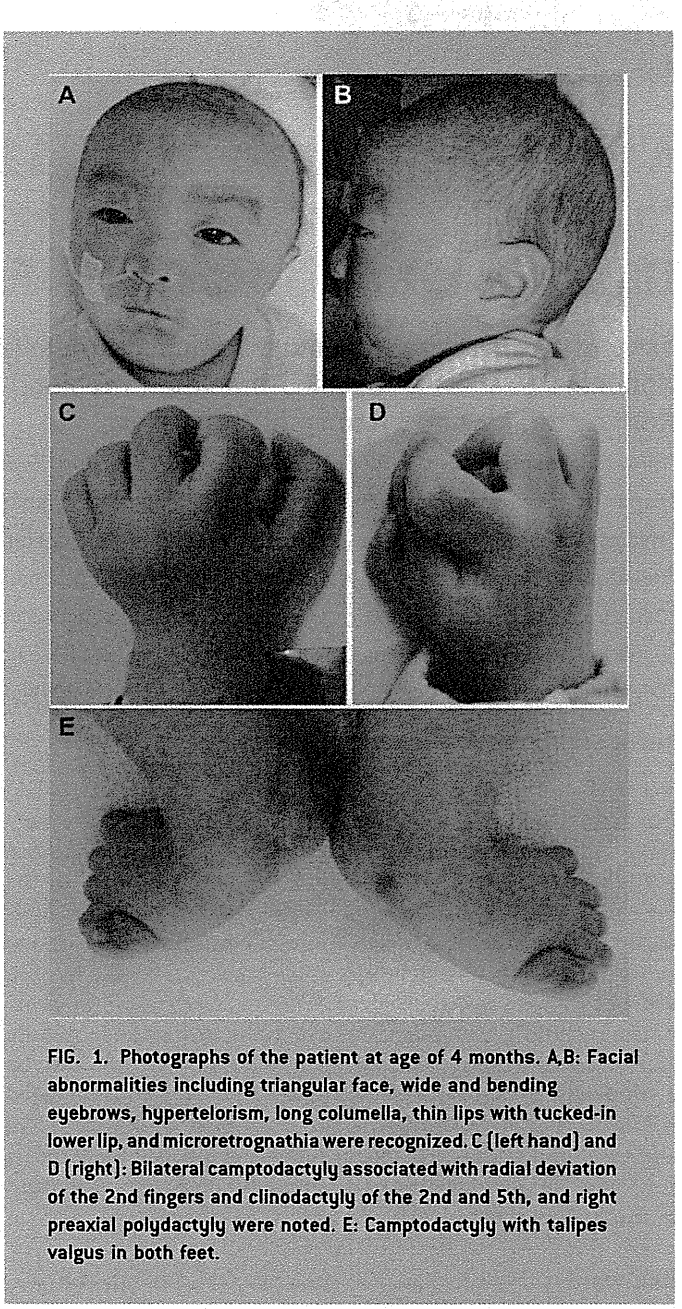

FIG. 1. Photographs of the patient at age of 4 months. A,B: Facial abnormalities including triangular face, wide and bending eyebrows, hypertelorism, long columella, thin lips with tucked-in lower lip, and microretrognathia were recognized. C (left hand) and D (right): Bilateral camptodactyly associated with radial deviation of the 2nd fingers and clinodactyly of the 2nd and 5th, and right preaxial polydactyly were noted. E: Camptodactyly with talipes valgus in both feet.

CYTOGENETIC AND MOLECULAR ANALYSIS

G-banded chromosomal analysis (550 bands level) of the patient's blood lymphocytes indicated normal karyptype (46,XY) (data not shown). Fluorescence in situ hybridization (FISH) analysis using all chromosomal subtelomeric clones did not show any abnormalities. Array CGH analysis using NimbleGen 385K Array (Roche NimbleGen, Inc., Madison, WI) demonstrated a 6.5-Mb heterozygous deletion at 20q11.2–q12 (UCSC genome coordinates 2006 Mar. version, chromosome 20: 31,269,661–37,782,841 bp) (Fig. 2A). The deletion was also confirmed by FISH using BACs (RP11-322B6 and RP11-782C16 at 21q11.21, and RP11-54P22 and RP11-467J15 at 20q12), RP11-787C16 and RP11-54P22 was deleted while RP11-322B6 and RP11-467J15 were not deleted (Fig. 3). The deletion junction was successfully amplified by PCR using primers (Primer A: 5′-TGA TAG AGC CAA CTG GGT CAT GTG C-3′, Primer C: 5′-TCT AGC TTG CTG AAT TCC TGC CTG A-3′) (Fig. 2B) and its product was sequenced. The deleted region was from 31,274,015 to 37,783,826 bp (6,509,811 bp) with 5-bp overlap (ATAGA) (Fig. 2C). The deletion occured de novo as FISH and

TABLE I. Clinical Manifestations of Reported Cases of 20q11–q12 Deletion

	Calliers' case (4 y, female)	Iqbals' case (2 y, male)	Present case (18 m, male)
General			
Growth retardation	+	+	+
Developmental delay	+	+	+
Autistic behavior	+	+	+
Sensory abnormalities/self-injury	+	+	+
Feeding difficulties	+	+	+
Gastroesophageal reflux	+	+	+
Gastrointestinal abnormalities	+ (Pyloric stenosis)	−	+ (Esophageal hiatus hernia)
Feeding intolerance	+ (Diarrhea, vomiting)	−	−
Dysphagia			+
Food refusal	+		+
Muscle tone	Hypertonia	Normal tone except for difficulty in extending the hips	Normal tone
Hearing loss		+	+
Congenital heart defect	−	−	+
Seizure/epilepsy		−	+
Central nervous system			
Cerebral atrophy	+	+	+
Craniofacial			
Triangular face	+	+	+
Hypertelorism	+	+	+
Hypoplastic alae nasi	+	+	+
Sparse hair	+		+
Down-slanting palpebral fissures	+		+
Long columella	+		+
Short, well-defined philtrum	+		+
Thin lips	+		+
Microretrognathia	+		+
Low-set ears	+		+
Extremities			
Arthrogryposis			+
Preaxial polydactyly			+
Clinodactyly of 5th fingers	+		+
Talipes equinovarus		+	
Talopes valgus			+
Ocular			
Retinal dysplasia			+
Microphthalmia		+	−
Duane anomaly		+	n.d.
Strabismus	+		−
Others			
Genital anomlies		+	−

Shadow indicates common features among three cases. y, year(s); m, month(s); +, positive; −, negative; n.d., not determined.

junction PCRs denied the deletion in parental samples (FISH data not shown and Fig. 2B by PCR using primers A, B, and C [primer B: 5′-AGC TGC TCA AAG TGG GGT ATT CTG G-3′]).

DISCUSSION

In this study, we precisely analyzed the 6.5-Mb deletion at 20q11.2–q12 in a boy, presenting with abnormal hands and feet, retinal dysplasia, and intractable feeding difficulty. Proximal interstitial deletions of 20q11–q12 are very rare. Only two cases have been reported and analyzed either by chromosomal CGH and FISH analysis or BAC array CGH with 1-Mb resolution [Callier et al., 2006; Iqbal and Al-Owain, 2007]. Clinical features are presented in Figure 1 and summarized in Table I. Three deletions are overlapping and the shortest region of overlap is from 20q11.22 to q11.23 (Fig. 3). Common clinical features among three cases are

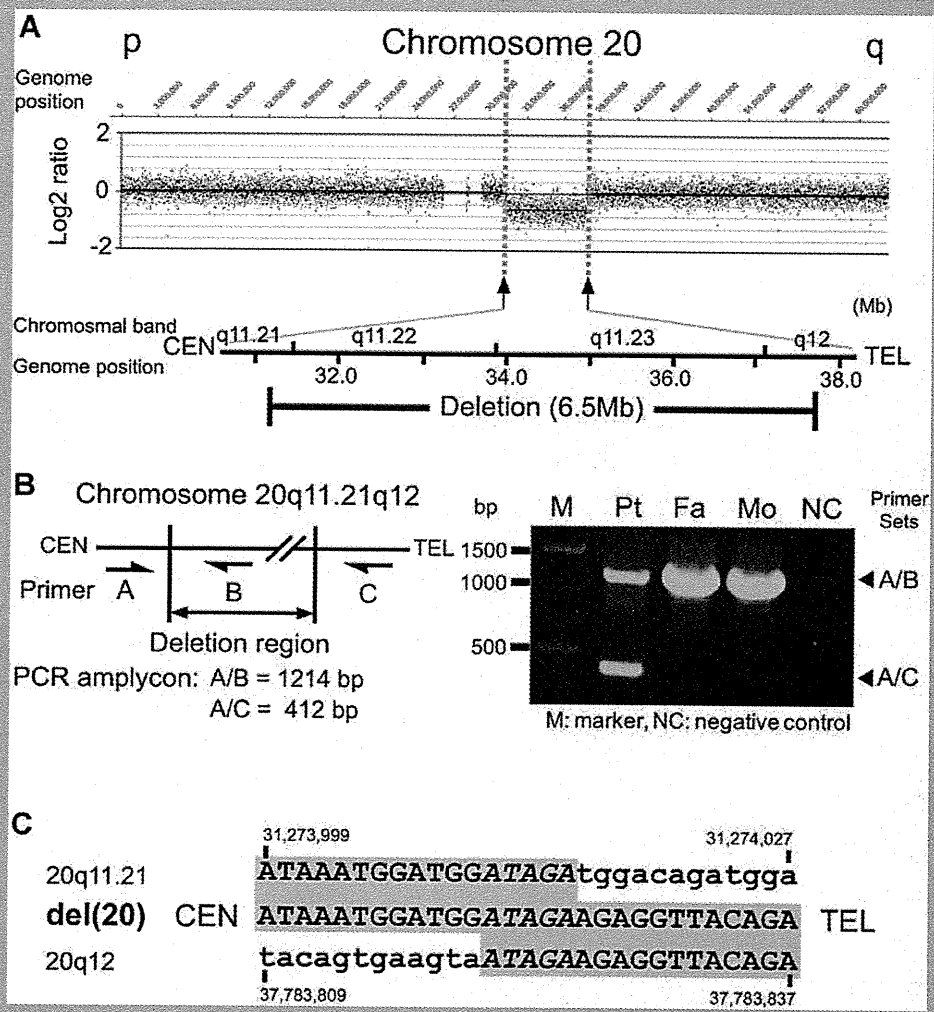

FIG. 2. Analysis of the 20q11.21–q12 deletion. A: High-resolution SNP array revealed the 6.5-Mb deletion at 20q11.21–q12. In the upper part, *Y* and *X* axes indicate probe signal intensity (log 2 ratio) and probe position in chromosome 20, respectively, and in the lower, chromosomal bands together with location of the deletion are shown. B: PCR system (left) to delineate the deletion and its result (right). C: Deletion junction sequence. Upper and lower sequences are normal ones around at proximal [20q11.21] and distal [20q12] deletion breakpoints, respectively. Middle shows the deletion junction in the patient. Gray shadow indicates matched sequences.

growth/developmental retardation, intractable feeding difficulties with GER, cerebral atrophy, and dysmorphic face including triangular face, hypertelorism, and hypoplastic alae nasi. In addition, two out of three patients shared many other facial dysmorphism including sparse hair, downslanting palpebral fissures, long columella, short and well-defined philtrum, thin lips, microretrognathia, and low-set ears. These findings suggest that the 20q11.22–q11.23 deletion can be a recognizable microdeletion syndrome. In addition, unique findings of hands and feet abnormalities as well as retinal dysplasia were found in our patient.

Intractable feeding difficulties in the three patients, is the largest concern for the family, and are speculated to be caused by combined factors: prolonged dysphagia (in our case), aspiration associated with GER (in all three), upper gastrointestinal tract abnormalties (pyloric stenosis [Callier et al., 2006] or esophageal hiatus hernia in our case), vomiting/diarrhea because of feeding intorerance [Callier et al., 2006], sensory abnormalities (in all), and food refusal (in the Callier et al. and our patient).

According to UCSC genome browser (March 2006 assembly), the 6.5-Mb deleted segment identified in our patient encompasses at least 96 known genes, including nine genes related to human disorders. One of these is growth/differentiation factor-5 (*GDF5*, also known as *CDMP1*). This is a protein which belongs to the GDF-subgroup of BMPs and plays an key regulatory role in embryonic skeletal and joint development. *GDF5* abnormalities are known to cause a variety of different skeletal disorders. Interestingly, Everman et al. [2002] and Yang et al. [2008] indicated that functional *GDF5* haploinsufficiency was the culprit of brachydactyly type C (BDC,

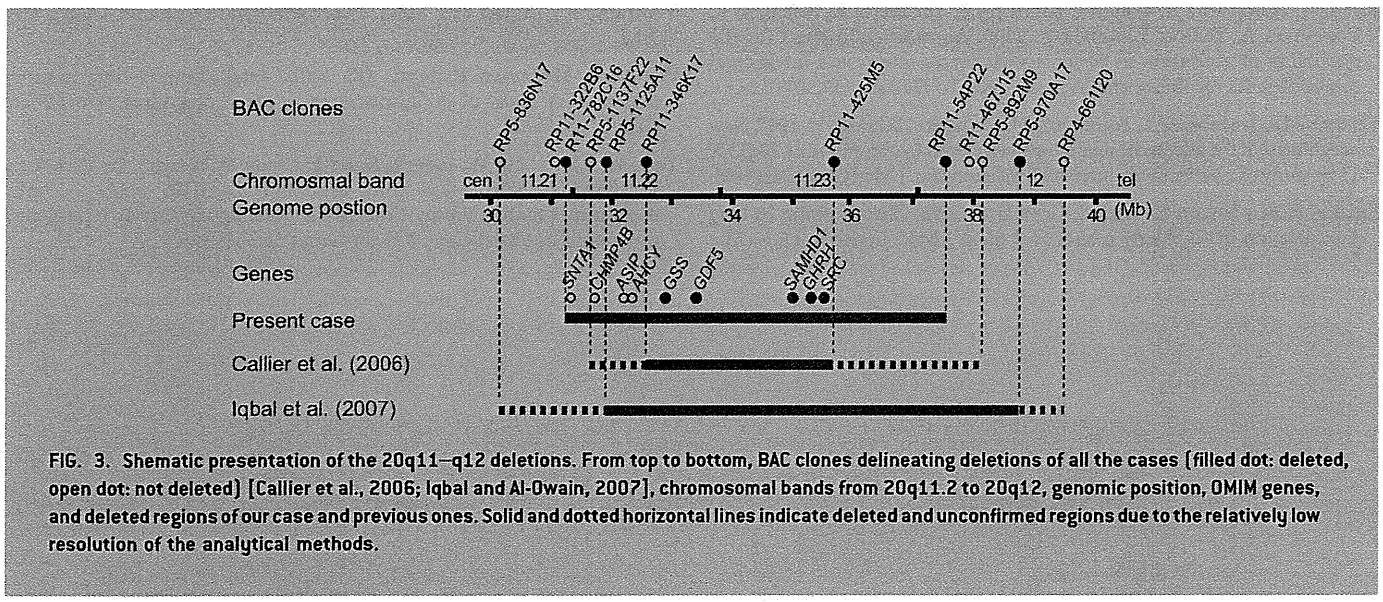

FIG. 3. Shematic presentation of the 20q11–q12 deletions. From top to bottom, BAC clones delineating deletions of all the cases [filled dot: deleted, open dot: not deleted] [Callier et al., 2006; Iqbal and Al-Owain, 2007], chromosomal bands from 20q11.2 to 20q12, genomic position, OMIM genes, and deleted regions of our case and previous ones. Solid and dotted horizontal lines indicate deleted and unconfirmed regions due to the relatively low resolution of the analytical methods.

OMIM #113100) by in vitro studies. As our patient has the *GDF5* haploinsufficiency, he may have the risk for BDC. However, he did not show this manifestation. He did have polydactyly, talipes valgus, and absence of the middle phalanges of the toes, which have been often found in individuals with BDC [Everman et al., 2002; Temtamy and Aglan, 2008]. Our patient did have a fetal akinesia (or hypokinesia) deformation phenotype (FADP). The short neck, hypertelorism, micrognathia, small thorax, postnatal respiratory disturbance, prolonged feeding difficulty, and slender long bone could represent FADP. FADP is a clinically and genetically heterogeneous constellation arising from fetal akinesia or decrease in utero movement due to intrinsic factors including neuropathy, myopathy, and restrictive dermopathy or extrinsic factors that limit fetal movement (e.g., tetragen exposure or fetal crowding) [Witters et al., 2002; Bamshad et al., 2009]. As extrinsic factors (e.g., abnormality of amniotic fluid, fetal crowding, congenital infection, and use of the drug in utero) could not be confirmed in this patient and the arthrogryposis and FADP are accompanied by other organ anomalies and developmental delay, the gene(s) at 20q11.21–q11.23 may be a primary intrinsic cause. Unfortunately, as skeletal malformations in the other two cases having the 20q11.2–q12 deletion were not fully described [Callier et al., 2006; Iqbal and Al-Owain, 2007], it is difficult to discuss the relationship between skeletal features and gene(s) in 20q11.2–q12 deletion.

Retinal dysplasia associated with falciform retinal fold and impaired vision was also noted. Retinal dysplasia is defined as abnormal growth and differentiation of embryonic retina either due to in utero environmental factors such as viral infection, tetragen exposure, retinopathy of prematurity or genetic factors. To our knowledge, this is the first description of retinal dysplasia associated with 20q11.2–q12 deletion.

ACKNOWLEDGMENTS

We are grateful to the patient and his family for their participation and support to this study. Grant-in Aid for Japan Society for the Promotion of Science (JSPS) Fellow (A.N.), Research Grants from the Ministry of Health, Labour and Welfare (N.M.), Grant-in-Aid from the Ministry of Education, Culture, Sports, Science and Technology of Japan (N.M.), and Grant-in-Aid for Scientific Research from JSPS (N.M.).

REFERENCES

Aldred MA, Aftimos S, Hall C, Waters KS, Thakker RV, Trembath RC, Brueton L. 2002. Constitutional deletion of chromosome 20q in two patients affected with albright hereditary osteodystrophy. Am J Med Genet 113:167–172.

Bamshad M, Van Heest AE, Pleasure D. 2009. Arthrogryposis: A review and update. J Bone Joint Surg Am 91:40–46.

Borozdin W, Graham JM Jr, Bohm D, Bamshad MJ, Spranger S, Burke L, Leipoldt M, Kohlhase J. 2007. Multigene deletions on chromosome 20q13.13-q13.2 including SALL4 result in an expanded phenotype of Okihiro syndrome plus developmental delay. Hum Mutat 28:830.

Callier P, Faivre L, Marle N, Thauvin-Robinet C, Sanlaville D, Gosset P, Prieur M, Labenne M, Huet F, Mugneret F. 2006. Major feeding difficulties in the first reported case of interstitial 20q11.22-q12 microdeletion and molecular cytogenetic characterization. Am J Med Genet Part A 140A:1859–1863.

Everman DB, Bartels CF, Yang Y, Yanamandra N, Goodman FR, Mendoza-Londono JR, Savarirayan R, White SM, Graham JM Jr, Gale RP, Svarch E, Newman WG, Kleckers AR, Francomano CA, Govindaiah V, Singh L, Morrison S, Thomas JT, Warman ML. 2002. The mutational spectrum of brachydactyly type C. Am J Med Genet 112:291–296.

Genevieve D, Sanlaville D, Faivre L, Kottler ML, Jambou M, Gosset P, Boustani-Samara D, Pinto G, Ozilou C, Abeguile G, Munnich A, Romana S, Raoul O, Cormier-Daire V, Vekemans M. 2005. Paternal deletion of the GNAS imprinted locus (including Gnasxl) in two girls presenting with severe pre- and post-natal growth retardation and intractable feeding difficulties. Eur J Hum Genet 13:1033–1039.

Iqbal MA, Al-Owain M. 2007. Interstitial del(20)(q11.2q12)—Clinical and molecular cytogenetic characterization. Am J Med Genet Part A 143A:1880–1884.

Kanda T, Murayama K, Kondo I, Kitazumi E, Takahashi K, Nakatani K, Yoneyama A, Yamori Y, Kanda Y. 2005. An estimation chart for the possibility of aspiration in patients with severe motor and intellectual disabilities: Its reliability and accuracy. No To Hattatsu 37:307–316.

Petersen MB, Tranebjaerg L, Tommerup N, Nygaard P, Edwards H. 1987. New assignment of the adenosine deaminase gene locus to chromosome 20q13 X 11 by study of a patient with interstitial deletion 20q. J Med Genet 24:93–96.

Shabtai F, Ben-Sasson E, Arieli S, Grinblat J. 1993. Chromosome 20 long arm deletion in an elderly malformed man. J Med Genet 30:171–173.

Temtamy SA, Aglan MS. 2008. Brachydactyly. Orphanet J Rare Dis 3:15.

Witters I, Moerman P, Fryns JP. 2002. Fetal akinesia deformation sequence: A study of 30 consecutive in utero diagnoses. Am J Med Genet 113:23–28.

Yang W, Cao L, Liu W, Jiang L, Sun M, Zhang D, Wang S, Lo WH, Luo Y, Zhang X. 2008. Novel point mutations in GDF5 associated with two distinct limb malformations in Chinese: Brachydactyly type C and proximal symphalangism. J Hum Genet 53:368–374.

RESEARCH ARTICLE

AMERICAN JOURNAL OF medical genetics PART A

Axenfeld–Rieger Anomaly and Axenfeld–Rieger Syndrome: Clinical, Molecular-Cytogenetic, and DNA Array Analyses of Three Patients With Chromosomal Defects at 6p25

Hidefumi Tonoki,[1,2]* Naoki Harada,[3] Osamu Shimokawa,[3] Ayako Yosozumi,[2] Kadomi Monzaki,[2] Kohei Satoh,[4] Rika Kosaki,[5] Atsushi Sato,[6] Naomichi Matsumoto,[7] and Susumu Iizuka[1]

[1]Section of Clinical Genetics, Department of Pediatrics, Tenshi Hospital, Sapporo, Japan

[2]Department of Pediatrics, Hokkaido University Graduate School of Medicine, Sapporo, Japan

[3]Kyushu Medical Science Nagasaki Laboratory, Nagasaki, Japan

[4]Department of Pediatrics, Sapporo Kousei Hospital, Sapporo, Japan

[5]Department of Clinical Genetics and Molecular Medicine, National Center for Child Health and Development, Okura, Setagaya-ku, Tokyo, Japan

[6]Faculty of Medicine, Department of Pediatrics, The University of Tokyo, Hongo, Bunkyo-ku, Tokyo, Japan

[7]Department of Human Genetics, Yokohama City University Graduate School of Medicine, Fukuura, Kanazawa-ku, Yokohama, Japan

Received 1 March 2010; Accepted 29 November 2010

Clinical phenotypes of and genetic aberrations in three unrelated Japanese patients with Axenfeld–Rieger anomalies and various accompanying malformations of systemic organs are described. GTG-banded chromosome analysis showed terminal deletions of the short arm of chromosome 6 in two patients and an inversion, inv(6)(p25q14), in the other. FISH and DNA array analyses revealed that the two patients with deletions had 5.0–5.7 Mb and 6.6 Mb 6p terminal deletions, respectively, and *FOXC1* was apparently deleted in both patients. In the other patient, the inversion breakpoint at 6p25 was estimated to be in or very close to the *FOXC1* locus, but DNA array analysis did not reveal a deletion around the breakpoint. Common extraocular findings in these patients included broad forehead, brachycephaly, hypertelorism, downslanting palpebral fissures, small anteverted nose, and cardiac defects. Two patients also exhibited autistic characteristics. The two patients with deletions exhibited poor muscle tone and developmental delays. Most of these extraocular findings were similar to those found in previous patients with *FOXC1* mutations and distinct from those found in patients with *PITX2* mutations, who frequently develop umbilical and dental anomalies. We suggest that the psychomotor retardation is a clinical manifestation associated with a deletion of multiple contiguous genes in the 6p terminus and that this phenomenon is similar to the 6p25 deletion syndrome. Understanding the relationship between genetic lesions and the spectrum of extraocular findings in patients with Axenfeld–Rieger anomalies may lead to better clinical management.

Key words: Axenfeld–Rieger anomaly; FOXC1; PITX2; DNA array; FISH; Rieger syndrome

How to Cite this Article:
Tonoki H, Harada N, Shimokawa O, Yosozumi A, Monzaki K, Satoh K, Kosaki R, Sato A, Matsumoto N, Iizuka S. 2011. Axenfeld–Rieger anomaly and Axenfeld–Rieger syndrome: Clinical, molecular-cytogenetic, and DNA array analyses of three patients with chromosomal defects at 6p25.
Am J Med Genet Part A 155:2925–2932.

INTRODUCTION

Axenfeld–Rieger anomalies, a group of genetically and phenotypically heterogeneous disorders leading to aberrant development of the anterior eye chambers, are frequently accompanied by a variety of major and minor anomalies of systemic organs, and patients with Axenfeld–Rieger anomalies have a 50% or higher incidence of

*Correspondence to:
Hidefumi Tonoki, M.D., Ph.D., Section of Clinical Genetics, Department of Pediatrics, Tenshi Hospital N-12, E-3, Sapporo 064-8611, Japan.
E-mail: hidefumi.tonoki@tenshi.or.jp
Published online 18 October 2011 in Wiley Online Library (wileyonlinelibrary.com).
DOI 10.1002/ajmg.a.33858

glaucoma [Fitch and Kaback, 1978; Alward, 2000]. Genetic loci associated with Axenfeld–Rieger anomalies have been mapped to three chromosomal regions: 4q25, 6p25, and 13q14 [Mears et al., 1996; Phillips et al., 1996; Semina et al., 1996a]. While the gene at 13q14 has not been identified, it is known that mutations in *PITX2* cause Axenfeld–Rieger anomalies mapping to 4q25 [Semina et al., 1996b] and that mutations in *FOXC1* underlie Axenfeld–Rieger anomalies mapping to 6p25 [Mears et al., 1998; Nishimura et al., 1998].

Historically, Axenfeld–Rieger anomalies and related conditions have been classified as Axenfeld anomaly, Rieger anomaly, or Rieger syndrome. Patients were considered to have Axenfeld anomaly when they presented with iris strands connecting the iridocorneal angel to the trabecular meshwork and a prominent, anteriorly displaced Schwalbe's line (posterior embryotoxon). If those patients presented with iris hypoplasia, corectopia (abnormal situation of pupil), or polycoria, they were considered to have Rieger anomaly. When these ocular findings were concurrent with facial, dental, or umbilical defects, patients were considered to have Rieger syndrome. However, the overlap in the spectrum of clinical manifestations and genetic heterogeneity in these patients makes this classification scheme somewhat confusing and has led to the proposal that these defects be classified as Axenfeld–Rieger anomaly (ARA) for patients presenting ocular defects only and Axenfeld–Rieger syndrome for patients with ocular and extraocular defects [Shields, 1983]. The term Axenfeld–Rieger anomalies is used to describe ARA with or without extraocular defects [Lines et al., 2002], but the correlation between the clinical and genetic findings in the subsets of patients has not been clearly established.

Here, we describe the clinical phenotypes of and genetic aberrations in three Japanese patients with ARA. Separate terminal deletions of chromosome 6p were found in two patients with phenotypes characteristic of so called Axenfeld–Rieger syndrome. The other patient who had congenial glaucoma and Rieger anomaly visited us asking whether his ocular anomaly was related to his abnormal karyotype: 46,XY,inv(6)(p25.1q12.1),t(4;12)(p25;q14).

CLINICAL REPORTS

This project was approved by the Committee for genetic test and counseling, Tenshi Hospital, Japan.

Patients

Patient 1. This Japanese girl was born after 42 weeks of gestation with a birth weight of 2,258 g (<5th centile), length of 47.4 cm (32nd centile), and head circumference of 33.0 cm (47th centile) to unrelated Japanese parents, who were both phenotypically normal.

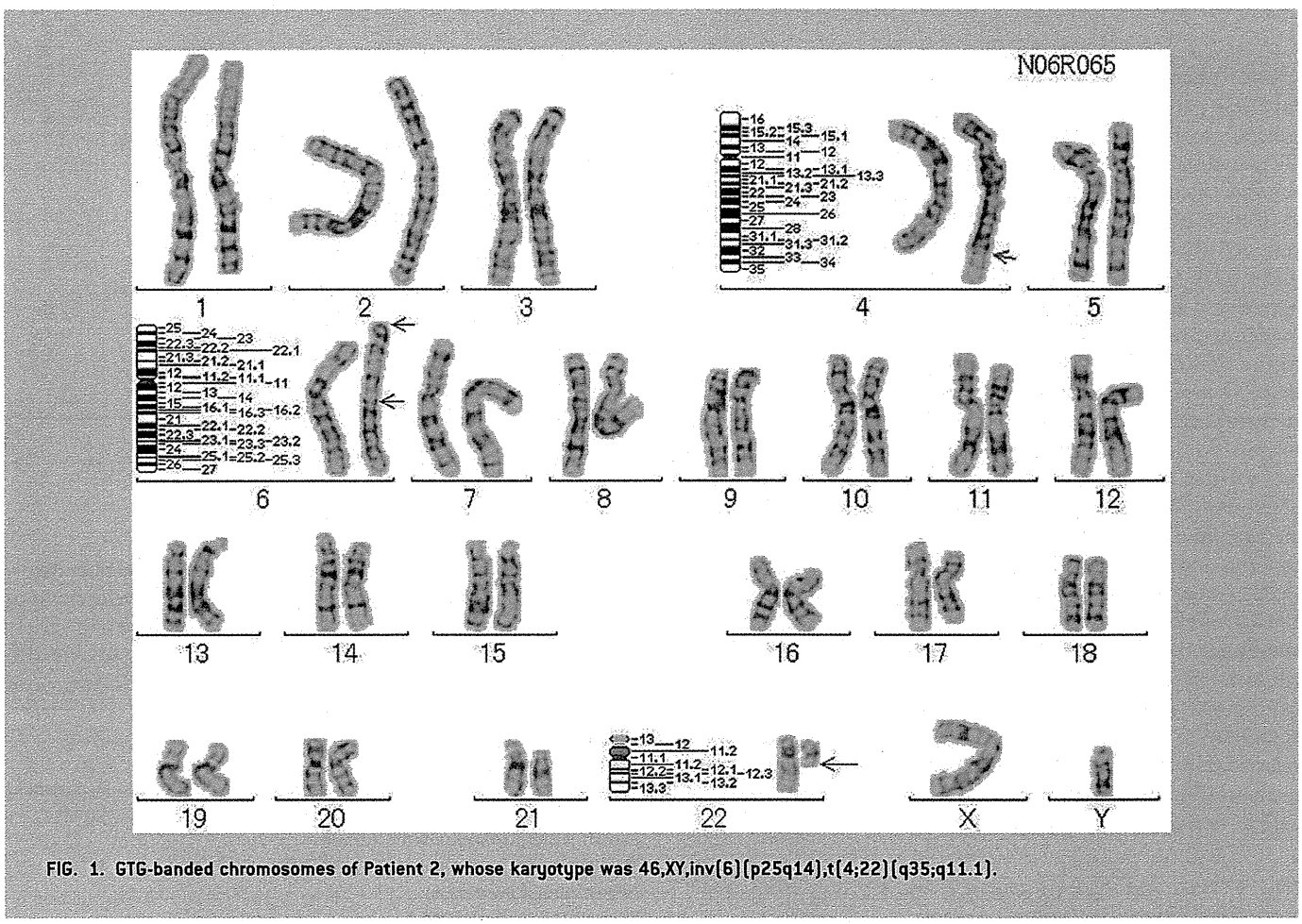

FIG. 1. GTG-banded chromosomes of Patient 2, whose karyotype was 46,XY,inv(6)(p25q14),t(4;22)(q35;q11.1).

She exhibited a number of congenital anomalies, including apparent hypertelorism, downslanting palpebral fissures, high palate, fusion of labia minor, redundant peri-umbilical skin, agenesis of corpus callosum, atrial septal defect, and bilateral sensorineural deafness. Ocular findings included buphthalmos in the neonatal period, posterior embryotoxon, and strabismus. Her intraocular pressure and pupil shape were normal, leading to a diagnosis of Axenfeld anomaly. Her developmental milestones were delayed; she controlled her head at 4 months of age, sat without support at 11 months, walked at 22 months, and had not spoken any meaningful words at 24 months. When measured at 19 months of age, her height was 80.2 cm (49th centile) and weight was 9.2 kg (21st centile). She showed autistic behavior at 5 years of age.

Standard G-banded chromosome analysis and multiple-chromosome painting revealed 46,XX,del(6)(p25.1). The karyotypes of the parents were normal.

Patient 2. This Japanese boy was born after 37 weeks of gestation with a weight of 2,926 g (64th centile), length of 48.0 cm (45th centile), and head circumference of 34.0 cm (62nd centile) to unrelated Japanese parents, who were phenotypically normal. In the neonatal period, he presented with cloudy cornea. Ophthalmological examination revealed that he had increased intraocular pressure, posterior embryotoxon, and iridogoniodysgenesis, leading to a diagnosis of Rieger anomaly. Chromosomal analysis showed an abnormal karyotype: 46,XY,inv(6)(p25q14),t(4;22)(q35;q11.1) (Fig. 1). When he visited us for genetic counseling at age 14 months he had a broad forehead and brachycephaly, apparent hypertelorism, downslanting palpebral fissures, maxillar hypoplasia, a small anteverted nose, and aortic coarctation. Dental, otic, or umbilical anomalies were not found. Audiologic examination did not reveal a hearing defect. Brain CT examination and ultrasound screening for abdominal organs were both normal. By the age of 2 years, he had undergone trabeculotomy and trabeculectomy on both eyes several times to control intraocular pressure. His growth and development were normal. He showed autistic behavior at 3 years of age. G-banded chromosomal analyses of the parents were normal.

Patient 3. This Japanese boy was born after 40 weeks of gestation with a birth weight of 3,230 g (56th centile), length of 49.1 cm (39th centile), and head circumference of 32.5 cm (28th centile) to unrelated Japanese parents, who were phenotypically normal. Atrial septal defect and pulmonary stenosis were found in the neonatal period, but no treatment was needed. Buphthalmos was noticed at 4 months of age. Ophthalmological examination revealed increased intraocular pressure and posterior embryotoxon. He was referred to us for genetic counseling at 8 months. He had a broad forehead, apparent hypertelorism, downslanting palpebral fissures, low-set and malformed ears, and a small anteverted nose. Brain MRI and brainstem auditory evoked potential were normal. No dental or umbilical anomalies were found. No surgery was necessary to treat the increased intraocular pressure. He was hypotonic, and his development was mildly delayed. His growth was normal. Chromosomal analysis revealed an abnormal karyotype: 46,XY,der(6)t(X;6)(p22.3;p25)dn. or 46,XY,der(6)t(Y;6)(p22.3;p25)dn. The karyotypes of the parents were normal.

METHODS

Chromosomal analysis was performed on peripheral blood lymphocytes. Metaphase chromosomes were G-banded for karyotype analysis and prepared for fluorescence in situ hybridization (FISH) analysis. RP-11 human BAC clones that map near the 6p25 breakpoints and the distal part of 6p were selected and utilized for FISH analysis, which was performed according to the standard protocol [Shimokawa et al., 2005]. Mapping information was retrieved from the UCSC genome browser, 2004 May version

TABLE I. FISH Results of Patients 1 and 2

		Position		FISH result	
Clone name	Band	Start	End	Patient 1	Patient 2
GS-62I11	6p25.3	Subtelomeric clone		Deletion	
RP11-139J12	6p25.3	74360	251686	Deletion	
RP11-939G22	6p25.3	924064	1099477	Deletion	Normal
RP11-10501	6p25.3	1099176	1279132		Normal
RP11-140F23	6p25.3	1304215	1456195		Normal
RP11-157J24	6p25.3	1372372	1547233		Normal
RP11-205J13	6p25.3	1456202	1625486	Deletion	Split
RP11-13F18	6p25.3	1462376	1633119		Split
RP11-964J7	6p25.3	1499784	1698745		Split
RP11-265E5	6p25.3	1562987	1723184		Inverted
RP11-452I2	6p25.3	1973365	2159947	Deletion	Inverted
RP11-420G6	6p25.2	2641239	2815840	Deletion	
RP11-349H3	6p25.1	4800266	4978093	Deletion	
RP11-324B14	6p25.1	5789659	5942278	Normal	
RP11-796J17	6p25.1	6331029	6531292	Normal	
RP11-69L16	6p24.3	7184568	7351773	Normal	
RP11-1065N24	6p24.2	11190385	11284706	Normal	

(http://genome.ucsc.edu/cga-bin/hgGateway). We also performed DNA array examination with Affymetrix GeneChip 250K Nsp array of 263,000 SNPs according to the manufacruer's protocols, and the data were analyzed using CNAG 3.0 software.

RESULTS

In Patient 1, FISH analyses using BAC clones, GS-62I11 (6p25.3), RP11-139J12 (6p25.3), RP11-939G22 (6p25.3), RP11-205J13 (6p25.3) (which encompasses the *FOXC1* gene), RP11-452I2 (6p25.3), RP11-452I2 (6p25.2), RP11-420G6 (6p25.2), and RP11-349H3 (6p25.1) resulted in a single spot of fluorescence. In contrast, hybridization with clones RP11-324B14 (6p25.1), RP11-796J17 (6p25.1), RP11-69L16 (6p24.3), and RP11-1065N24 (6p24.2) resulted in two fluorescent signals (Table I and Fig. 2). These results were confirmed by a comparative genomic hybridization study that revealed a 5.0–5.7 Mb 6p terminal deletion (data not shown).

In Patient 2, three *FOXC1*-containing clones, RP11-205J13, RP11-13F18, and RP11-265E5, gave split signals on the inv(6)chromosome, while clones distal and proximal to *FOXC1* gave signals at the original position and at the inverted position, respectively (Table I and Fig. 2). DNA array analysis revealed no loss or gain of signals on any part of chromosomes 6 (Fig. 3a), 4, or 22 (data not shown).

In Patient 3, DNA array tests revealed a 6,610 kb deletion of the short arm of chromosome 6 encompassing SNP A-2058596 (position 119,769) to SNP A-1892272 (position 6,735,864) (Fig. 3b).

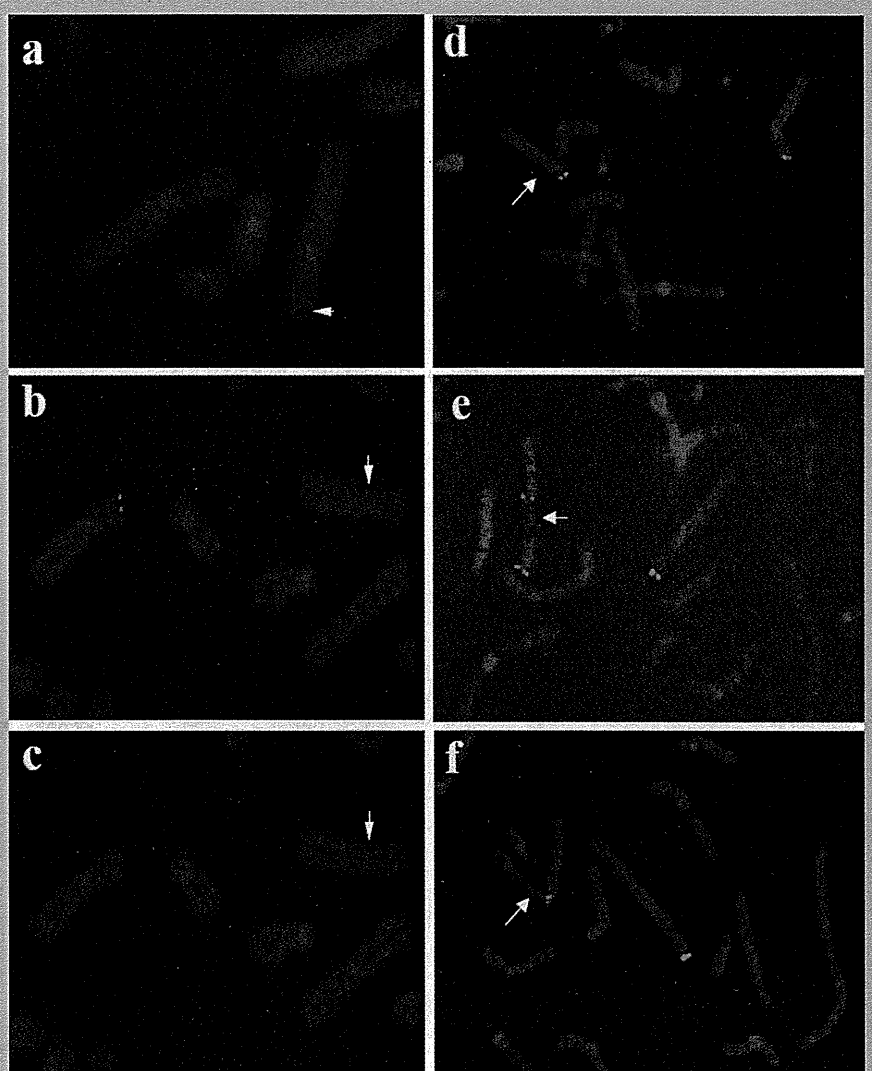

FIG. 2. FISH analysis of Patient 1 with BAC clones. RP11-205J13 on 6p25.3 (a) and clone RP11-349H3 on 6p25.1 (b) did not give any signal on del(6)(arrow). RP11-324B14 (c) on 6p25.1 gave a signal on del(6) (arrow). FISH analysis of Patient 2 (d,e), with BAC clones RP11-157J24 (d), RP11-13F18 (e), and RP11-265E5 (f), showing distal, split, and proximal (inverted position) signals, respectively, on inv(6). [Color figure can be seen in the online version of this article, available at http://onlinelibrary.wiley.com/journal/10.1002/(ISSN)1552-4833]

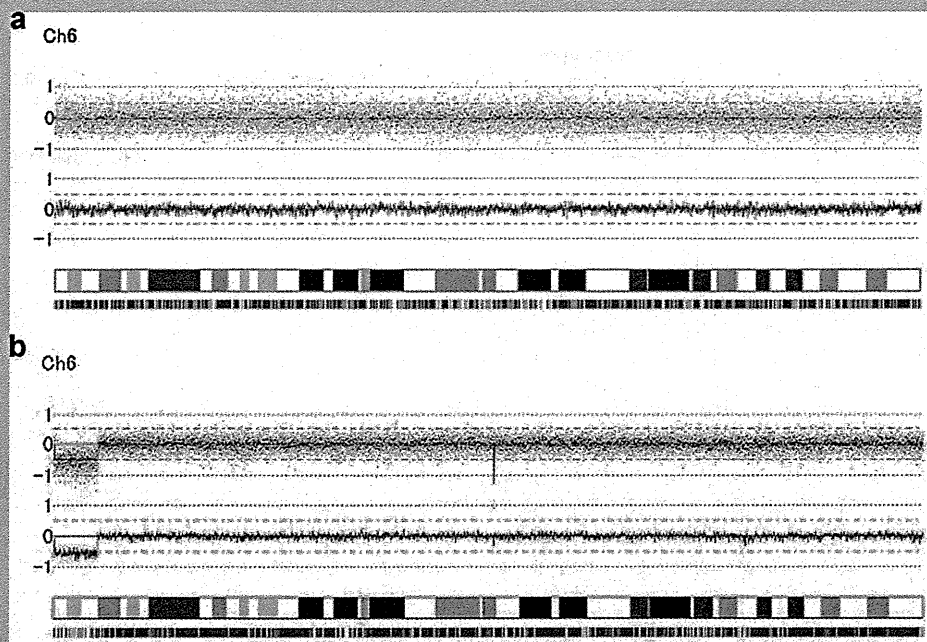

FIG. 3. DNA array examination with Affymetrix mapping 250K array for 263,000 SNPs in Patients 2 and 3. These data were analyzed using GTC and CNAG software, revealing no loss or gain of signals of chromosome 6 in Patient 2 (a) and 6.61 kb deletion of terminal region of the short arm of chromosome 6 in Patient 3 (b). [Color figure can be seen in the online version of this article, available at http://onlinelibrary.wiley.com/journal/10.1002/(ISSN)1552-4833]

DISCUSSION

We analyzed the genomic lesions in three patients with ARA. The FISH analyses and DNA array examinations along with G-banded chromosome analyses clearly showed a 5.0–5.7 Mb and a 6.6 Mb 6p terminal deletion in Patients 1 and 3, respectively (Fig. 4). *FOXC1* coding sequence is located at position 1555680–1557341 in 6p25.3, and the gene was apparently deleted both in Patients 1 and 3. In Patient 2, the results of FISH analyses and DNA array examination indicated that the chromosomal breakpoint at 6p25.3 was in or very close to the *FOXC1* locus (Fig. 4). Therefore, it is plausible that in Patient 2 the breakpoint at 6p25.3 directly interrupted the gene structure or somehow impaired the function of *FOXC1* through a position effect, similar to that in a patient with a balanced translocation, t(6;13)(p25.3;q22.3) [Nishimura et al., 1998].

Several patients with 6p terminal deletions have been reported [Kume et al., 1998; Law et al., 1998; Nishimura et al., 1998; Baruch and Erickson, 2001; Lehmann et al., 2002; Anderlid et al., 2003; Maclean et al., 2005; Suzuki et al., 2006; Martinez-Glez et al., 2007; Martinet et al., 2008]. Recently, Gould et al. [2004] and Lin et al. [2005] summarized the phenotypes of patients with 6p25 deletions, showing that these patients exhibited a recognizable pattern of malformations, namely 6p25 deletion syndrome. These malformations include hypertelorism, downslanting palpebral fissures, ARA, hearing loss, anomalies in the central nervous system, and developmental delay. As shown in Table II, manifestations of Patients 1 and 3 were consistent with those of the 6p25 deletion

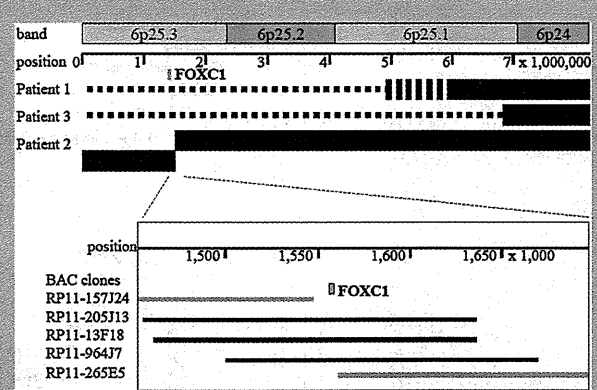

FIG. 4. Diagram of the chromosomal aberrations in Patients 1, 2, and 3. The dotted bars indicate the extent of the 6p terminal deletions in Patients 1 and 3. In Patient 2, slippage of the boxes indicates the breakpoint. In the lower box, locations of *FOXC1* and some of the BAC clones used to analyze samples from Patient 2 are shown. *FOXC1* is located between BAC clones RP11-157J24 and RP11-265E5, which gave the signals at the normal and inverted position, respectively, on Inv(6). Three BAC clones that gave split signals on Inv(6) overlap each other and contain *FOXC1*.

TABLE II. Summary of Clinical Findings in Patients With 6p25 Anomalies

	This report			Nishimura et al.	Gould et al.	Lin et al.
	P1	P3	P2	First patient	19 cases	9 cases[b]
	6p25 deletion					
Chromosomal anomaly[a]			Inv	TB	6p25 deletion	6p25 deletion
Anterior chamber defect	+	+	+	+	17/19	7/9
Broad forehead and brachycephaly	+	+	+			
Hypertelorism	+	+	+	+	12/14	7/8
Downslanting palpebral fissures	+	+	+			6/7
Small/anteverted nose	+	+	+			
Palatal anomaly	+	−	−	+		
Dental anomalies	−	−	−			
Ear anomalies	−	+	−			4/8
Hearing loss	+	−	−		14/15	6/8
Umbilical anomalies	+	−	−			1/4
Structural CNS anomaly	+	−	−	+	8/14	3/5
Cardiac defects	+	+	+		9/14	6/8
Hypoplastic lungs	−	−	−	+		
Genitourinary anomaly	+	−	−			1/2
Poor muscle tone	+	+	−			3/4
Developmental delay	+	+	−			9/9

P2, Patient 2; P3, Patient 3; P1, Patient 1 in this report.
+, present; −, not present; blank, not reported.
[a]Inv inv(6)(p25q14), TB: t(6;13)(p25.3;q22.3).
[b]Three cases were also reviewed by Gould et al.

syndrome. Most of the clinical manifestations in these patients were thought to be due to haploinsufficiency of multiple genes in the 6p terminal region. Patient 2 in this study and a patient reported by Nishimura et al. [1998] each had a balanced chromosomal rearrangement and exhibited diverse multiple extraocular findings; for example, Patient 2 exhibited apparent hypertelorism, downslanting of palpebral fissures, maxillar hypoplasia, and aortic coarctation, while the patient from the previous report exhibited hypertelorism, palatal anomaly, CNS anomaly, and hypoplastic lungs. The diversity of these phenotypes suggests that chromosome breakage at

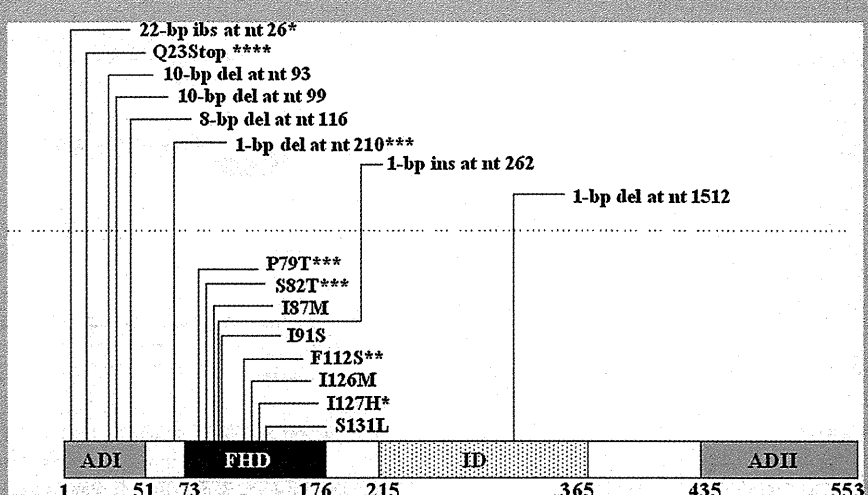

FIG. 5. Schematic representation of previously reported *FOXC1* mutations and associated phenotypes. Boxes represent FOXC1 domains, and the numbers indicate amino acid positions. ADI, activation domain I; FHD, forkhead domain; ID, inhibitory domain; and ADII, activation domain II. The truncation mutations are above dotted line, and the missense mutations are below it. Symbols on the right shoulder of mutation indicate that patients carrying the mutation had the following extraocular findings: *, hypertelorism; **, dental anomaly; ***, cardiac anomaly; ****, hypertelorism and dental, umbilical, and cardiac anomalies.

6p25 in those two patients might influence the function of *FOXC1* and other neighboring genes because most patients with simple *FOXC1* mutations had only intraocular abnormalities. The array of *FOXC1* mutations with which clinical phenotype are documented is shown in Figure 5 [Mears et al., 1998; Nishimura et al., 1998, 2001; Swiderski et al., 1999; Mirzayans et al., 2000; Kawase et al., 2001; Suzuki et al., 2001]. Of the 70 patients with documented *FOXC1* mutations, 8 patients had hypertelorism, and 7 had cardiac anomalies. These two phenotypes may be relatively frequent in patients with *FOXC1* mutations. In contrast, dental and umbilical defects were frequently observed in ARA patients with *PITX2* mutations, and hypertelorism and cardiac anomalies were rarely seen in these patients [Semina et al., 1996b; Schinzel et al., 1997; Alward et al., 1998; Flomen et al., 1998; Kulak et al., 1998; Doward et al., 1999; Perveen et al., 2000; Priston et al., 2001; Saadi et al., 2001; Semina, 2004]. Although actual frequencies of extraocular dysmorphic features associated with of Rieger syndrome have not been established, umbilical and dental anomalies seem to accompany *PITX2* defects frequently, while hypertelorism and cardiac anomalies are often associated with *FOXC1* defects. This difference in the spectrum of extraocular phenotypes between *FOXC1* and *PITX2* lesions could be due to differences in tissue-specific expression of *PITX2* versus *FOXC1* [Semina et al., 1996b; Nishimura et al., 1998].

Understanding the relationship between the genetic lesions and clinical manifestations in patients with Axenfeld–Rieger syndrome would provide better clinical management and genetic evaluation, but this relationship is a complex and difficult matter. Further studies on the function(s) of two genes, *FOXC1* and *PITX2*, or other unrecognized genes in the 6p25 region are necessary.

REFERENCES

Alward WL. 2000. Axenfeld–Rieger syndrome in the age of molecular genetics. Am J Ophthalmol 130:107–115.

Alward WL, Semina EV, Kalenak JW, Héon E, Sheth BP, Stone EM, Murray JC. 1998. Autosomal dominant iris hypoplasia is caused by a mutation in the Rieger syndrome (RIEG/PITX2) gene. Am J Ophthalmol 125:98–100.

Anderlid BM, Schoumans J, Hallqvist A, Stahl Y, Wallin A, Blenow E, Nordenskjold M. 2003. Cryptic subtelomeric 6p deletion in a girl with congenital malformations and severe language impairment. Eur J Hum Genet 11:89–92.

Baruch AC, Erickson R. 2001. Axenfeld–Rieger anomaly, hypertelorism, clinodactyly, and cardiac anomalies in sibs with an unbalanced translocation der(6)t(6;8). Am J Med Genet 100:187–190.

Doward W, Perveen R, Lloyd IC, Ridgway AE, Wilson L, Black GC. 1999. A mutation in the RIEG1 gene associated with Peters' anomaly. J Med Genet 36:152–155.

Fitch N, Kaback M. 1978. The Axenfeld syndrome and the Rieger syndrome. J Med Genet 15:30–34.

Flomen RH, Vatcheva R, Gorman PA, Baptista PR, Groet J, Barisić I, Ligutic I, Nizetić D. 1998. Construction and analysis of a sequence-ready map in 4q25: Rieger syndrome can be caused by haploinsufficiency of RIEG, but also by chromosome breaks approximately 90 kb upstream of this gene. Genomics 47:409–413.

Gould DB, Jaafar MS, Addison MK, Munier F, Ritch R, MacDonald IM, Walter MA. 2004. Phenotypic and molecular assessment of seven patients with 6p25 deletion syndrome: Relevance to ocular dysgenesis and hearing impairment. BMC Med Genet 5:17.

Kawase C, Kawase K, Taniguchi T, Sugiyama K, Yamamoto T, Kitazawa Y, Alward WL, Stone EM, Nishimura DY, Sheffield VC. 2001. Screening for mutations of Axenfeld–Rieger syndrome caused by FOXC1 gene in Japanese patients. J Glaucoma 10:477–482.

Kulak SC, Kozlowski K, Semina EV, Pearce WG, Walter MA. 1998. Mutation in the RIEG1 gene in patients with iridogoniodysgenesis syndrome. Hum Mol Genet 7:1113–1117.

Kume T, Deng KY, Winfrey V, Gould DB, Walter MA, Hogan BL. 1998. The forkhead/winged helix gene Mfl is disrupted in the pleiotropic mouse mutation congenital hydrocephalus. Cell 93:985–996.

Law CJ, Fisher AM, Temple IK. 1998. Distal 6p deletion syndrome: A report of a case with anterior chamber eye anomaly and review of published reports. J Med Genet 35:685–689.

Lehmann OJ, Ebenezer ND, Ekong R, Ocaka L, Mungall AJ, Fraser S, McGill JI, Hitchings RA, Khaw PT, Sowden JC, Povey S, Walter MA, Bhattacharya SS, Jordan T. 2002. Ocular developmental abnormalities and glaucoma associated with interstitial 6p25 duplications and deletions. Invest Ophthalmol Vis Sci 43:1843–1849.

Lin RJ, Cherry AM, Chen KC, Lyons M, Hoyme HE, Hudgins L. 2005. Terminal deletion of 6p results in a recognizable phenotype. Am J Med Genet Part A 136A:162–168.

Lines MA, Kozlowski K, Walter MA. 2002. Molecular genetics of Axenfeld–Rieger malformations. Hum Mol Genet 11:1177–1184.

Maclean K, Smith J, St Heaps L, Chia N, Williams R, Peters GB, Onikul E, McCrossin T, Lehmann OJ, Adès LC. 2005. Axenfeld–Rieger malformation and distinctive facial features: Clues to a recognizable 6p25 microdeletion syndrome. Am J Med Genet Part A 132A:381–385.

Martinet D, Filges I, Schmutz NB, Morris MA, Gaide A-C, Dahoun S, Bottani A, Addor M-C, Antonarakis SE, Beckmann JS, Bena F. 2008. Subtelomeric 6p deletion: Clinical and array-CGH characterization in two patients. Am J Med Genet Part A 146A:2094–2102.

Martinez-Glez V, Lorda-Sanchez I, Ramirez JM, Ruiz-Barnes P, Rodriguez de Alba M, Diego-Alvarez D, Ramos C, Searby CC, Nishimura DY, Ayuso C. 2007. Clinical presentation of a variant of Axenfeld–Rieger syndrome associated with subtelomeric 6p deletion. Eur J Med Genet 50:120–127.

Mears AJ, Mirzayans F, Gould DB, Pearce WG, Walter MA. 1996. Autosomal dominant iridogoniodysgenesis anomaly maps to 6p25. Am J Hum Genet 59:1321–1327.

Mears AJ, Jordan T, Mirzayans F, Dubois S, Kume T, Parlee M, Ritch R, Koop B, Kuo WL, Collins C, Marshall J, Gould DB, Pearce W, Carlsson P, Enerbäck S, Morissette J, Bhattacharya S, Hogan B, Raymond V, Walter MA. 1998. Mutations of the forkhead/winged-helix gene, FKHL7, in patients with Axenfeld–Rieger anomaly. Am J Hum Genet 63:1316–1328.

Mirzayans F, Gould DB, Heon E, Billingsley GD, Cheung JC, Mears AJ, Walter MA. 2000. Axenfeld–Rieger syndrome resulting from mutation of the FKHL7 gene on chromosome 6p25. Eur J Hum Genet 8:71–74.

Nishimura DY, Swiderski RE, Alward WL, Searby CC, Patil SR, Bennet SR, Kanis AB, Gastier JM, Stone EM, Sheffield VC. 1998. The forkhead transcription factor gene FKHL7 is responsible for glaucoma phenotypes which map to 6p25. Nat Genet 19:140–147.

Nishimura DY, Searby CC, Alward WL, Walton D, Craig JE, Mackey DA, Kawase K, Kanis AB, Patil SR, Stone EM, Sheffield VC. 2001. A spectrum of FOXC1 mutations suggests gene dosage as a mechanism for developmental defects of the anterior chamber of the eye. Am J Hum Genet 68:364–372.

Perveen R, Lloyd IC, Clayton-Smith J, Churchill A, van Heyningen V, Hanson I, Taylor D, McKeown C, Super M, Kerr B, Winter R, Black GC. 2000. Phenotypic variability and asymmetry of Rieger syndrome

associated with PITX2 mutations. Invest Ophthalmol Vis Sci 41:2456–2460.

Phillips JC, del Bono EA, Haines JL, Pralea AM, Cohen JS, Greff LJ, Wiggs JL. 1996. A second locus for Rieger syndrome maps to chromosome 13q14. Am J Hum Genet 59:613–619.

Priston M, Kozlowski K, Gill D, Letwin K, Buys Y, Levin AV, Walter MA, Héon E. 2001. Functional analyses of two newly identified PITX2 mutants reveal a novel molecular mechanism for Axenfeld–Rieger syndrome. Hum Mol Genet 10:1631–1638.

Saadi I, Semina EV, Amendt BA, Harris DJ, Murphy KP, Murray JC, Russo AF. 2001. Identification of a dominant negative homeodomain mutation in Rieger syndrome. J Biol Chem 276:23034–23041.

Schinzel A, Brecevic L, Dutly F, Baumer A, Binkert F, Largo RH. 1997. Multiple congenital anomalies including the Rieger eye malformation in a boy with interstitial deletion of (4) (q25 → q27) secondary to a balanced insertion in his normal father: Evidence for haplotype insufficiency causing the Rieger malformation. J Med Genet 34:1012–1014.

Semina EV. 2004. PITX2 and PITX3 and the Axenfeld–Rieger syndrome, Iridogoniodysgenesis and iris hypoplasia, Peters anomaly, and anterior segment ocular dysgenesis. In: Epstein CJ, Erickson RP, Wynshaw-Boris A, editors. Oxford monographs on medical genetics no. 49, Molecular basis of developmental malformations. New York: Oxford University Press. pp. 599–606.

Semina EV, Datson NA, Leysens NJ, Zabel BU, Carey JC, Bell GI, Bitoun P, Lindgren C, Stevenson T, Frants RR, van Ommen G, Murray JC. 1996a. Exclusion of epidermal growth factor and high-resolution physical mapping across the Rieger syndrome locus. Am J Hum Genet 59:1288–1296.

Semina EV, Reiter R, Leysens NJ, Alward WL, Small KW, Datson NA, Siegel-Bartelt J, Bierke-Nelson D, Bitoun P, Zabel BU, Carey JC, Murray JC. 1996b. Cloning and characterization of a novel bicoid-related homeobox transcription factor gene, RIEG, involved in Rieger syndrome. Nat Genet 14:392–399.

Shields MB. 1983. Axenfeld–Rieger syndrome: A theory of mechanism and distinctions from the iridocorneal endothelial syndrome. Trans Am Ophthalmol Soc 81:736–784.

Shimokawa O, Miyake N, Yoshimura T, Sosonkina N, Harada N, Mizuguchi T, Kondoh S, Kishino T, Ohta T, Remco V, Takashima T, Kinoshita A, Yoshiura K, Niikawa N, Matsumoto N. 2005. Molecular characterization of del(8)(p23.1p23.1) in a case of congenital diaphragmatic hernia. Am J Med Genet Part A 136A:49–51.

Suzuki T, Takahashi K, Kuwahara S, Wada Y, Abe T, Tamai M. 2001. A novel (Pro79Thr) mutation in the FKHL7 gene in a Japanese family with Axenfeld–Rieger syndrome. Am J Ophthalmol 132:572–575.

Suzuki K, Nakamura M, Amano E, Mokuno K, Shirai S, Terasaki H. 2006. Case of chromosome 6p25 terminal deletion associated with Axenfeld–Rieger syndrome and persistent hyperplastic primary vitreous. Am J Med Genet Part A 140A:503–508.

Swiderski RE, Reiter RS, Nishimura DY, Alward WL, Kalenak JW, Searby CS, Stone EM, Sheffield VC, Lin JJ. 1999. Expression of the Mfl gene in developing mouse hearts: Implication in the development of human congenital heart defects. Dev Dyn 216:16–27.

SHORT REPORT

Rapid detection of a mutation causing X-linked leucoencephalopathy by exome sequencing

Yoshinori Tsurusaki,[1] Hitoshi Osaka,[2] Haruka Hamanoue,[1] Hiroko Shimbo,[2] Megumi Tsuji,[2] Hiroshi Doi,[1] Hirotomo Saitsu,[1] Naomichi Matsumoto,[1] Noriko Miyake[1]

[1]Department of Human Genetics, Yokohama City University Graduate School of Medicine, Yokohama, Japan
[2]Division of Neurology, Clinical Research Institute, Kanagawa Children's Medical Center, Yokohama, Japan

Correspondence to
Dr Noriko Miyake, Department of Human Genetics, Yokohama City University Graduate School of Medicine, 3-9 Fukuura, Kanazawa-ku, Yokohama 236-0004, Japan;
nmiyake@yokohama-cu.ac.jp

Received 20 October 2010
Revised 14 December 2010
Accepted 5 February 2011
Published Online First 17 March 2011

ABSTRACT

Background Conventional PCR-based direct sequencing of candidate genes for a family with X-linked leucoencephalopathy with unknown aetiology failed to identify any causative mutations.

Objective To carry out exome sequencing of entire transcripts of the whole X chromosome to investigate a family with X linked leucoencephalopathy.

Methods and results Next-generation sequencing of all the transcripts of the X chromosome, after liquid-based genome partitioning, was performed on one of the two affected male subjects (the proband) and an unaffected male subject (his brother). A nonsense mutation in *MCT8* (c.1102A→T (p.R368X)) was identified in the proband. Subsequent PCR-based direct sequencing of other family members confirmed the presence of this mutation, hemizygous in the other affected brother and heterozygous in the proband's mother and maternal grandmother. *MCT8* mutations usually cause abnormal thyroid function in addition to neurological abnormalities, but this proband had normal thyroid function.

Conclusion Single-lane exome next-generation sequencing is sufficient to fully analyse all the transcripts of the X chromosome. This method is particularly suitable for mutation screening of X-linked recessive disorders and can avoid biases in candidate gene choice.

INTRODUCTION

High-throughput, next-generation sequencing (NGS) can have a tremendous impact on human genetic research.[1] Even personal whole-genome analysis is possible,[2] but the cost of obtaining and analysing an entire genome from many people is still unrealistic for many laboratories. Selection and enrichment of regions of interest (genome partitioning) enable us to use NGS efficiently for reasonable numbers of patients with genetic disorders.[3–6]

Ready-to-use microarray-based and solution-based hybridisation systems are now commercially available. A combination of genome partitioning using these systems and NGS is one of the most promising ways to identify genes causing Mendelian disorders.[3 4 6]

Here, we performed exome sequencing of entire transcripts of the whole X chromosome to investigate a family with X linked leucoencephalopathy with unknown aetiology after intensive candidate gene analysis by conventional exon-by-exon Sanger sequencing. A single-lane run of NGS on only two family members successfully determined the leucoencephalopathy-causing mutation.

SUBJECTS AND METHODS

A family with X-linked leucoencephalopathy

The proband (III-2) was a 13-year-old boy. He was born to Japanese consanguineous parents (II-3, 4) after an uneventful pregnancy (figure 1A). His birth weight was 3440 g. Congenital horizontal nystagmus was noted as a neonate. Because of his poor weight gain and developmental delay, he was referred to us at age 5 months. He showed progressive spasticity and dystonia with exaggerated deep tendon reflexes as well as myoclonic and tonic seizures, which responded to valproic acid and clonazepam at age 21 months. Brain MRI at 2 years showed diffuse hyperintensity of the frontal lobe on T2-weighted images, suggesting hypomyelination, and normal T1-weighted images (figure 1B,C). The peak latency intervals in auditory brainstem responses (I–V/III–V) were 4.63/2.37 ms, which were elongated compared with those of age-matched controls (4.24±0.08/1.97±0.08 ms (mean±SD)). He was clinically diagnosed with Pelizaeus–Merzbacher disease (MIM#312080), although neither mutation nor duplication was found in *PLP1* (RefSeq Gene ID, NM_000533) or *GJA12* (NM_020435) (the duplication in *GJA12* was not checked). He was never able to follow objects or control his head.

The dystonia worsened and he is now mechanically ventilated because of tracheomalacia. A thyroid function test at age 13 years indicated all normal levels: free tri-iodothyronine (T_3) 1.2 ng/ml (normal range 0.8–1.6 ng/ml), free thyroxine (T_4) 6.4 μg/dl (normal range 6.1–12.4 μg/dl) and thyroid-stimulating hormone 1.2 μIU/ml (normal range 0.5–5 μIU/ml). Brain MRI at age 13 years demonstrated improvement of myelination in the white matter, but he still presented with severe mental retardation (figure 1D,E). His younger brother was an 8-year-old boy (III-3) with an almost identical clinical course and MRI findings. His grandparents (I-1, I-2) were both healthy. The elder uncle (II-1) died at age 27 years who, initially, could walk with support but who declined towards the end of his life. Another uncle (II-2) was diagnosed with cerebral palsy and died at 7 months of age of unknown causes.

Informed consent was obtained from the patient's family members in accordance with human study protocols approved by the

J Med Genet 2011;**48**:606–609. doi:10.1136/jmg.2010.083535

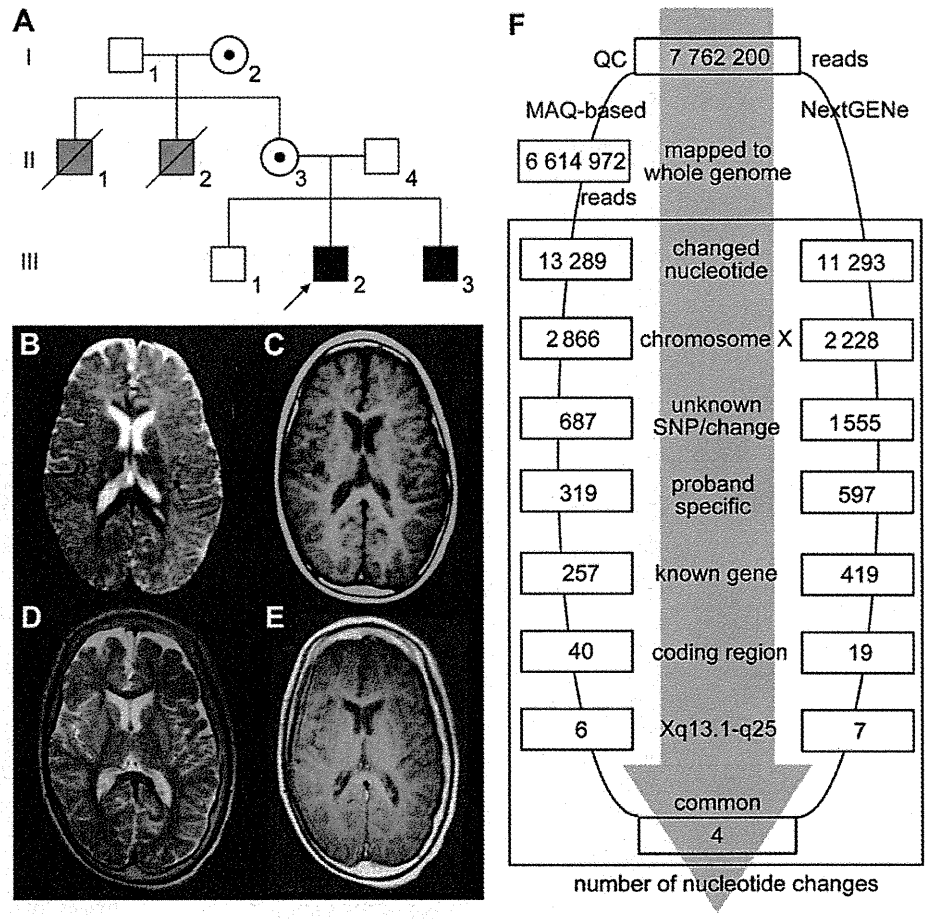

Figure 1 Pedigree and brain MRI of the proband. (A) Family pedigree. (B) T2-weighted image at age 2 years shows diffuse hyperintensity, especially in the frontal lobe. (C) T1-weighted image at 2 years shows nearly complete myelination. (D and E) At age 13 years, both T2 (D) and T1 (E)-weighted images demonstrate complete myelination; the hypomyelination observed at age 2 years can therefore be regarded as delayed myelination. (F) Flow of informatics analysis. A MAQ-based method and NextGENe analysis were performed (III-2). The selection methods included variation relative to the human genome reference sequence; variants mapped to the X chromosome; unknown variants (excluding registered SNPs); variants identified in the proband only (not in his healthy brother); variants in known genes; coding region variants; variants in genes at Xq13.1–q25; and variants common to the two informatics methods. MAQ, Mapping and Assembly with Qualities; SNP, single nucleotide polymorphism.

institutional review board at Kanagawa Children's Medical Centre and Yokohama City University School of Medicine.

Genome-wide single nucleotide polymorphism (SNP) genotyping

Genome-wide SNP genotyping was undertaken for individuals I-1, I-2, II-3, II-4, III-1, III-2 and III-3 using the GeneChip Human Mapping 10K Array *Xba* 142 2.0 (Affymetrix Inc, Santa Clara, California, USA), according to the manufacturer's protocols. Mendelian errors in the pedigree to exclude conflicted SNPs were checked using GeneChip operating software 1.2 (Affymetrix) and batch analysis in GeneChip genotyping analysis software 4.0 (Affymetrix), with the default settings for a mapping algorithm. Copy Number Analyzer for GeneChip 2.0 was used to validate copy number alterations.[7] The linked region with SNPs shared between individuals III-2 and III-3 (not observed in III-1) was checked manually.

Genome partitioning, short-read sequencing and sequence alignment

Genomic DNAs from the proband (III-2) and his unaffected brother (III-1) were used for this study. Three micrograms of DNA were processed using a SureSelect X chromosome test kit (1582 transcripts covering 3053 kb) (Agilent Technologies, Santa Clara, California, USA), according to the manufacturer's instructions. Captured DNAs were analysed using an Illumina GAIIx (Illumina Inc, San Diego, California, USA). We used only one of the eight lanes of the flow cell (Illumina), performing single 76 bp reads for each sample. Image analysis and base calling were performed by sequence control software (SCS) real-time analysis (Illumina) and/or offline Basecaller software v1.6 (Illumina) and CASAVA software v1.6 (Illumina). Reads were aligned to the human reference genome sequence (UCSC hg18, NCBI build 36.1) using the ELAND v2 program (Illumina). Coverage was calculated statistically. Identified variants were annotated based on novelty, impact on the encoded protein, the number and frequency of reads and conservation. NextGENe software v1.99 (SoftGenetics, State College, Pennsylvania, USA) was also used to analyse reads, with the default settings.

Mapping strategy and variant annotation

Approximately 9.9 million reads from III-1 (the unaffected sibling) and 7.8 million reads from III-2 (the proband), which passed the quality control (Path Filter), were mapped to the human reference genome by Mapping and Assembly with Qualities (MAQ)[8] and NextGENe software (SoftGenetics) (figure 1F). The bait region of the X chromosome based on the manufacturer's information was carefully evaluated. MAQ was able to align 7 359 688 and 6 614 972 reads to the whole genome for III-1 and III-2, respectively, which were statistically analysed for coverage using a script created by BITS Co Ltd (Tokyo, Japan). SNPs and indels were extracted from the alignment data using another script created by BITS, along with information on registered SNPs (dbSNP build 130). A consensus quality score of ≥40 was used for the SNP analysis in MAQ.

Capillary sequencing

Possible pathological variants were confirmed by Sanger sequencing using an ABI 3500xl or ABI3100 autosequencer (Life Technologies, Carlsbad, California, USA), following the manufacturer's protocol. Sequencing data were analysed by

Sequencher software (Gene Codes Corporation, Ann Arbor, Michigan, USA).

RESULTS AND DISCUSSION

Coverage analysis showed that 78.9% of all the X chromosome transcripts were completely covered by reads, and that 11.6% of transcripts were at least 90% covered. Almost all (99%) of these regions were covered by 20 reads or more (100 reads or more in 97%) by only single-lane sequencing. SNP genotyping was able to delineate the minimal linked region from rs763739 to rs1073455 (UCSC genome browser hg19 assembly, X chromosome coordinates: 76 804 990–126 844 262) (50 Mb). The maximum linked region was from rs1926354 to rs859587 (UCSC genome browser coordinates: 68 404 915–128 933 907) (60.5 Mb). Exome GAIIx sequencing with the two informatics methods identified four potentially interesting changes in the maximum linked region: c.1102AT (p.R368X) in *MCT8* (NM_006517; alternatively called *SLC16A2*); c.1402T→G (p.S468A) and c.1943A→G (p.H648R) in *CYLC1* (NM_021118); and c1606G→A (p.D536N) in *LRCH2* (NM_020871) (figure 1F). c.1102A→T (p.R368X) in *MCT8* was found heterozygously in the proband's healthy mother (II-3) and maternal grandmother (I-2), and hemizygously in the proband and his affected younger brother; each was confirmed by Sanger sequencing (figure 2). This change was not present among 92 normal female controls (0/184 alleles).

The *MCT8* gene encodes a thyroid hormone transporter and is implicated in syndromic X-linked mental retardation, Allan–Herndon–Dudley syndrome and Pelizaeus–Merzbacher-like disease (PMLD).[9–12] This nonsense mutation, c.1102A→T (p.R368X), which might lead to nonsense-mediated decay resulting in no protein production, is highly likely to be pathological. Based on the human gene mutation database (http://www.hgmd.cf.ac.uk/ac/index.php), three nonsense mutations in this gene have been previously registered: p.R245X, p.Q335X and p.S448X. The other identified variants, in *CYLC1* and *LRCH2*, are all SNPs because they were identified in normal controls: c.1402T→G (*CYLC1*): 5/182 alleles, c.1943A→G (*CYLC1*): 12/184 alleles and c1606G→A (*LRCH2*): 5/184 alleles. We concluded that the *MCT8* mutation was pathogenic in this family.

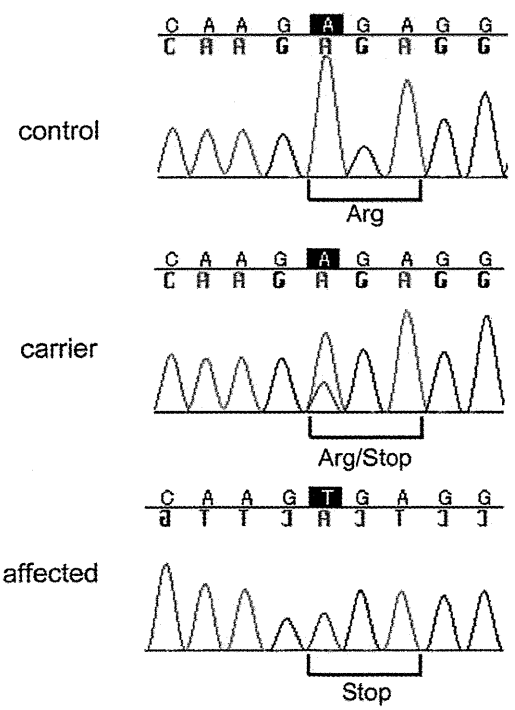

Figure 2 Electropherograms of a normal control, a carrier (mother) and the affected proband.

PMLD caused by *MCT8* mutations presents with infantile hypotonia, severe psychomotor development, nystagmus, generalised muscle weakness, dystopia, joint contracture and progressive spastic paraplegia. All affected male subjects develop the disease, while heterozygous female subjects are clinically normal or sometimes show mild thyroid dysfunction.[9 12] Brain MRI shows delayed myelination in the first few years of life, which subsequently improves but with residual neurological disability. The unique diagnostic feature of the disease is an abnormal thyroid hormone profile: increased free T_3, decreased free T_4 and normal thyroid-stimulating hormone.[12] The cases we analysed here showed clinical features and brain MRI findings typical of PMLD, but no thyroid hormone abnormalities. Based on regular laboratory testing and conventional PCR-based gene screening, we might have failed, or taken much longer, to identify the causative mutation. Thus, unbiased screening without prior knowledge is one of the advantages of NGS.

Thyroid hormone (T_4 and T_3) is important in neuronal development and its deficiency in the pre/neonatal stage causes a form of mental retardation called cretinism. T_4 is released from the thyroid as a prohormone and is altered to biologically active T_3 by iodothyronine deiodinases.[13] Active T_3 is delivered to the peripheral organs via thyroid hormone transporters. MCT8 is a thyroid hormone-specific transporter and is mainly expressed in the brain and liver.[14 15] In MCT8 deficiency, T_3 and T_4 uptake is impaired and deiodinase 2 is activated.[16] This results in increased serum T_3 levels because of T_3 accumulation in the peripheral blood. In previous reports, the majority of patients showed abnormal levels of thyroid hormones, but some displayed values within the normal range.[9 10 12 17 18] The variable range for abnormal thyroid hormone levels might be explained by unidentified modifier effect(s) and/or other transporter(s) that can compensate for MCT8 function.[19] Additionally, although MCT8 deficiency has been determined by abnormalities in thyroid function tests, it is unknown what proportion of the patients with MCT8 deficiency show abnormal thyroid function. We suggest that it is important to evaluate thyroid hormone function in PMLD with unknown cause.

Before the exome NGS analysis, we screened *PLP1*, *GJA12*, and seven other candidate genes mapped to the linked region: *MSN* (NM_002444), *IGBP1* (NM_001551), *SNX12* (NM_013346), *OGT* (NM_181672), *HDAC8* (NM_018486), *SH3BGRL* (NM_003022.2) and *PCDH11X* (NM_032967.2). Because we found no pathological changes, we adopted the exome sequencing strategy. We determined that exome sequencing with a single lane for each sample was sufficient to analyse all the transcripts of the X chromosome. In X-linked recessive diseases, male subjects are usually affected, and therefore the single X chromosome is the primary target of exome sequencing. Except for mosaic mutations, the hemizygous (rather than heterozygous) status of disease-related nucleotide changes is relatively easy to detect using all-or-none NGS reads (0% or 100% of reads). There was no difference in the ability of our two informatics methods (MAQ and NextGENe) to detect pathological changes. This approach could equally be applied to the analysis